PAPER

Identification of large channels in cationic PEGylated cubosome nanoparticles by synchrotron radiation SAXS and Cryo-TEM imaging

Borislav Angelov,[a] Angelina Angelova,*[b] Markus Drechsler,[c] Vasil M. Garamus,[d] Rada Mutafchieva[e] and Sylviane Lesieur[b]

Extra-large nanochannel formation in the internal structure of cationic cubosome nanoparticles results from the interplay between charge repulsion and steric stabilization of the lipid membrane interfaces and is evidenced by cryogenic transmission electron microscopy (Cryo-TEM) and synchrotron radiation small-angle X-ray scattering (SAXS). The swollen cubic symmetry of the lipid nanoparticles emerges through a shaping transition of onion bilayer vesicle intermediates containing a fusogenic nonlamellar lipid. Cationic amphiphile cubosome particles, thanks to the advantages of their liquid crystalline soft porous nanoarchitecture and capability for multi-drug nanoencapsulation, appear to be of interest for the design of mitochondrial targeting devices in anti-cancer therapies and as siRNA nanocarriers for gene silencing.

Introduction

The possibility to engineer the water channel networks in bicontinuous liquid crystalline (LC) cubic lipid phases characterizes them as adaptive supramolecular nanomaterials, permitting the encapsulation, transport and delivery of various kinds of active ingredients.[1–6] Several macromolecular drugs (peptides, proteins, and siRNA) have been successfully encapsulated in cubosomal nanostructures and chief membrane proteins have been crystallized in lipid cubic phases.[4] Both kinetic pathways and structure formation in soft mesoporous materials present strong ongoing research interest towards understanding of the biomolecular loading, migration, and release from amphiphile- and lipid-based LC nanoarchitectures.[2a,5–14] Conn *et al.* have demonstrated a remarkable order of structural transformations upon application of temperature or pressure jump stimuli in monoglyceride (monoelaidin)/water self-assembled systems.[7a]

Bicontinuous lipid cubic phases with large water channels (channel size bigger than 6 nm) have been evidenced by small angle X-ray scattering (SAXS).[8c–g] Their inner LC architecture involves organized 3D lipid membrane labyrinths that separate intertwined networks of water-swollen channel compartments.[10,11] Large water nanochannels represent a protein-friendly environment for either water-soluble or membrane anchored proteins.[2a,c,3b,4,6b] Almsherqi *et al.* have discovered biomembranes of cubic symmetries with considerably swollen nanochannels (cubic lattice size of up to 500 nm) in samples of biological origin.[14a] This fact has suggested that aqueous channel formation on the mesoscale has important biological significance in health and disease states. As a matter of fact, the same cubic membrane type is present over different length scales. In any case, the structure of the cubic biomembranes *in vivo* has been characterized by essentially larger channel dimensions as compared to those of the self-assembled bicontinuous cubic phases of model lipids.[6–9]

Augmented water channel diameters may facilitate the accommodation of hydrophilic biomacromolecules (*e.g.* siRNA, DNA, or peptides) in synthetic drug delivery nanocarriers. Practically, the nanochannel size should be increased, through a decrease of the lipid membrane curvature,[8b] in order for a supercoiled plasmid DNA (a stiff dumbbell-like shape) to penetrate into the water-channel network of the lipid cubic assembly. The amount of water taken up upon swelling of the LC structures can be modulated through the functionalization of the lipid membrane/water interfaces (*e.g.* by inclusion of charged lipid components and hydration agents).[2b,5c,6b,9–12] The work of Engblom *et al.*[8f] has proposed

[a] *Institute of Macromolecular Chemistry, Academy of Sciences of the Czech Republic, Heyrovskeho Nam. 2, 16206 Prague, Czech Republic*

[b] *CNRS UMR8612 Institut Galien Paris-Sud, Univ Paris Sud, LabEx LERMIT, Châtenay-Malabry, F-92296 France. E-mail: Angelina.Angelova@u-psud.fr*

[c] *Laboratory for Soft Matter Electron Microscopy, Bayreuth Institute of Macromolecular Research, University of Bayreuth, D-95440 Bayreuth, Germany*

[d] *Helmholtz-Zentrum Geesthacht, Centre for Materials and Coastal Research, D-21502 Geesthacht, Germany*

[e] *Institute of Biophysics and Biomedical Engineering, Bulgarian Academy of Sciences, BG-1113 Sofia, Bulgaria*

controlling the sizes of the water channels in mixed cubic lipid phases by varying the content of the anionic lipid in the studied nonlamellar lipid mixtures.

Cubic LC lipid particles (cubosomes) can be fabricated by two major approaches. The first one consists of "top-down" fragmentation of bulk mesophases of lyotropic amphiphiles,[3,9] while the second one is based on "bottom-up" assembly of vesicular membranes.[2d,6c,8a] A question, which remains open in the context of the "top-down" approach, is whether the Pluronic polymer shell (providing long circulation of the cubosome nanoparticles)[9a] might ensure or hamper the diffusion of biomacromolecules in/out the nanochannelled carriers. This concern should be minor upon utilization of PEGylated lipids for cubic nanoparticle dispersion.[2d,3d,6e]

It has been shown that unilamellar vesicles generated by self-assembly of nonlamellar lipids may pack into tetrahedral-type channel architectures through a membrane fusion mechanism.[6c,8a] The resulting precursors of water-filled cubic channel networks favour a vesicle-to-cubosome nanoparticle transition.[6c,8a,9c,11a] Notably, Yaghmur et al.[11a,e] have induced a vesicle-to-cubosome transition by injecting Ca$^+$ ions to the dispersed lipid system or by means of temperature variations in the presence of the polymeric stabilizer F127, which has been suggested to play a role in the membrane fusion process.

The ongoing interest in cationic liquid crystalline lipid nanocarriers is motivated by the enhanced capacity of the cubosomes for encapsulation of guest biomolecules and also by the possibility for their targeting. In this work, we consider that the nanochannel size tuning and large pore formation in such particles can be governed by electrostatic repulsion of the bicontinuous lipid membrane/water interfaces. Moreover, PEGylation of the interfaces may impart membrane flexibility and may ensure steric stabilization of the designed nanostructured carriers. We investigate the mechanism of formation of water-swollen channels of cubic symmetry within individual PEGylated cubosome nanoparticles. This fundamental problem requires elucidation from a structural view point.

Results and discussion

Here we report extra-large nanochannel formation in cationic lipid cubosome particles stabilized by PEGylation. Cryogenic transmission electron microscopy (Cryo-TEM) and SAXS were employed to reveal the nanochannelled inner organization of the LC nanocarriers. A fully hydrated self-assembled lipid mixture of monoolein (MO), dioctadecyldimethylammonium bromide (DOMA), and 1,2-dioleoyl-sn-glycero-3-phospho-ethanolamine-N-(methoxy(polyethyleneglycol)-2000) ammonium salt (DOPE-PEG$_{2000}$) was dispersed in excess aqueous phosphate buffer medium in order to generate positively charged PEGylated LC membrane-type nanoparticles.

For Cryo-TEM analysis of the cationic nanocarriers, several images were taken from the nanoparticles solution in order to obtain representative structural information. Fig. 1(a)–(c) reveal that the created positively charged cubosome intermediates are
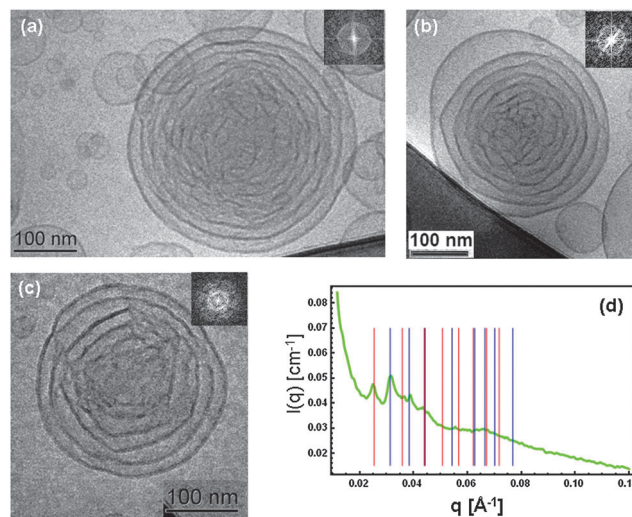

Fig. 1 (a)–(c) Cryo-TEM images of cationic lipid cubosome intermediates with extra-large water channels (FFT are given as insets). (d) SAXS pattern of the same sample demonstrating the coexistence of Pn3m (double diamond) (blue bars representing the sequence $\sqrt{2}:\sqrt{3}:\sqrt{4}:\sqrt{6}:\sqrt{8}:\sqrt{9}:\sqrt{10}$ of peak positions) and Im3m (primitive) inner cubic lattice structures (red bars indicating the sequence $\sqrt{2}:\sqrt{4}:\sqrt{6}:\sqrt{8}:\sqrt{10}:\sqrt{12}:\sqrt{14}:\sqrt{16}$ of peak positions). The nanoparticle sample composition is derived from MO/DOMA/DOPE-PEG$_{2000}$ (82/15/3 mol%) LC membranes dispersed in excess buffer medium. The SAXS pattern (d) is representative of scattering from dispersed nano-objects with the internal liquid crystalline structure. It differs from a diffraction pattern of a bulk lipid mixture.

stable in excess aqueous medium and have particle diameters of about 300 nm. Their inner core bicontinuous cubic structure involves large water-filled nanochannels. An onion-like organization is easily resolved starting from the peripheries of the nanoparticles. A fraction of small vesicles and nanocubosomes[6c,e] is present in the nonlamellar lipid dispersion in order to maintain the thermodynamic equilibrium of the lipid membranes at ambient temperature. It has been suggested[6c,8a] that onion intermediates and bilayer stacks are a prerequisite for the induction and growth of cubic nanochannel network structures in lipid membrane nanoparticles. Similar "rose-like" intermediates have been recently observed during a composition-mediated cubic phase transition upon preparation of fluorescent cubosomes for theranostic applications.[9e]

Fig. 1(d) shows the SAXS pattern characterizing the organization of the cationic lipid nanoparticles in excess buffer medium. Coexisting inner cubic structures of Pn3m (double diamond) and Im3m (primitive) symmetries were identified upon indexing of the diffraction peaks. The sequences of the first eight peaks for each LC nanostructure were analyzed. On the basis of the SAXS data, the following extra large lipid cubic lattice parameters were determined in excess water phase: a_{Pn3m} = 28.3 nm and a_{Im3m} = 34.9 nm. Using the constant lipid bilayer thickness model proposed by Clerc, Dubous-Violette, Garstecki and Hołyst,[15d,e] the diameter of the water channels ($D_w \sim$ 13 nm) and the membrane bilayer thickness (L = 6.2 nm) were determined. Since the membrane of the pure monoolein cubic phase has a thickness of $\sim$3.2 nm, the variation of 3 nm should be attributed to
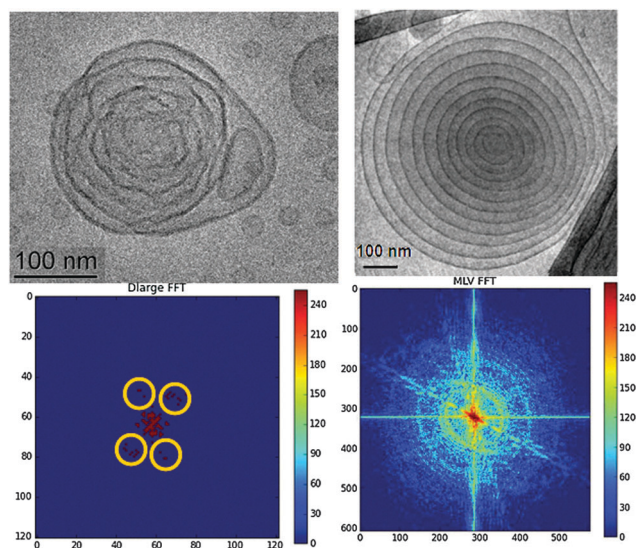
the associated coverage of PEG chains at the lipid membrane interface. This result confirms that the investigated dispersion is homogeneous and that it does not contain a nondispersed bulk lipid phase.

It should be noted that the number of repeat unit cells in the studied lipid nanoparticles is insufficient for a long range order to develop as it may occur in low hydrated bulk nonlamellar lipid assembly. Therefore, the SAXS pattern is rather a result of the form and structure factors related to the lipid membrane shaping and internal structuring in the cubosome intermediates. The fast Fourier transforms (FFT) of the Cryo-TEM images (Fig. 1(a)–(c)) also indicate nonisotropic structures resembling the early structural stages of formation of cubosome nanoparticles.

Towards interpretation of the obtained raw Cryo-TEM data, and finding a connection with the SAXS results (Fig. 1), FFT analysis was performed in the context of a "bottom-up" structural transition from lamellar lipid bilayer arrangements to cubic-membrane packing and ordering. The first step of the geometrical consideration of the inner nanoparticle structure consisted in identification of the individual lipid membranes that begin to fold before entering into a cubic phase transition.

Fig. 2 presents the topologies of the initial (top right) and the final (top left panel) states of the structural transition from a multilamellar onion-bilayer stack to a cubic lipid membrane nanoparticle with large water channels. The folding of the bilayer membranes in the investigated nanocarriers is suggested to be driven by the nonlamellar propensity of the self-assembled amphiphilic mixture. Both steric repulsive undulations[9d] of the interfaces (provoked by their PEGylation) and modulation of the charge repulsion[2b] (introduced by the cationic lipid component DOMA) are involved in the nanoobject shaping.

The performed FFT of the Cryo-TEM images are shown in Fig. 2 (bottom row). They reveal a notable structural difference between the onion bilayer particle (right panel) and the monoolein-based cationic lipid carrier, which undergoes a cubic transformation (left panel). Evidently, the investigated onion-bilayer topological transformation process takes place through a lamellar-to-cubic mesophase transition rather than by virtue of unilamellar vesicles aggregation.[6c] This result supports our observation that the number of inner lipid bilayers in the onion-like stacks should be greater than five in order to allow for the initiation of a cubic transition in such soft multilamellar onions.[11b] Interestingly, confinement of five inner lipid bilayers in multi-component amphiphilic nanoparticles has favoured the formation of pear-type and elongated onion shapes.[11b] The established deformations of the lipid/water interfaces likely resulted from inhomogeneous curvature distribution along the membranes. This effect may not be excluded taking into account the employed low percentage of the PEGylated lipid (3 mol%). The latter is insufficient to homogeneously cover the entire membrane surface by PEG chains. The embedded PEGylated lipid tends to locally reduce the curvature of the nonlamellar lipid assembly.[1c] Moreover, it may preferentially partition, due to its hydrophilic nature, at the nanoparticle periphery, which explains the prevalence of low-curvature (onion-like) membranes at the nanocarrier outer side. The obtained structural result confirms the higher degree of hydration of the nanocarrier periphery exposed to the excess water environment.

The second step of the Cryo-TEM image analysis focused on the presence of a nanoparticle core of an inner cubic nanostructure in the cationic lipid carriers. The lipid membranes turn up with fluctuating shapes in the Cryo-TEM image of the studied large-channel cubosomal intermediates (Fig. 2, top left panel). The nonsmooth shapes reveal the inhomogeneous curvature distribution along the lipid/water interfaces during the geometric transformation. The folding bilayers become condensed into a symmetric supramolecular architecture with discernable peaks reminiscent of a cubic packing (highlighted yellow circles in Fig. 2, bottom left panel). The smearing of the peaks was attributed to the small number of unit cells in the swollen-type cubosome carrier, the membrane fluctuations, and the low statistics that may be expected for just one cubosome particle. At variance, the FFT pattern, plotted in the bottom right panel of Fig. 2, revealed arc-shaped peaks typical for multilamellar vesicles.[13]

We assume that the coexistence of primitive Im3m and diamond Pn3m cubic symmetries in the SAXS pattern in Fig. 1(d) likely results from the form factors characterizing every sufficiently large cubosomic intermediate that is present in the lipid dispersion. A SAXS pattern corresponding to a mixture of two separate structure factors of well-defined bulk-like cubosome aggregates of these symmetries would be less appropriate for description of the obtained experimental results. Taking into account the recently reported structural findings for multiphase and multicompartment lipid nanoparticles,[8a] it follows that multiphase nanostructures may readily form in dispersed liquid crystalline nanocarriers due

Fig. 2 (top) Cryo-TEM images presenting a topological comparison between a cubosome precursor particle with very large aqueous channels (left) and a multilamellar lipid vesicle (right). The scale bar in the images is 100 nm. (bottom) Corresponding fast Fourier transformations (FFT) of the Cryo-TEM images with cubic lattice peaks on the left panel highlighted by yellow circles. The percentage of the cationic lipid is 15 mol% (left panel) and 25 mol% (right panel).
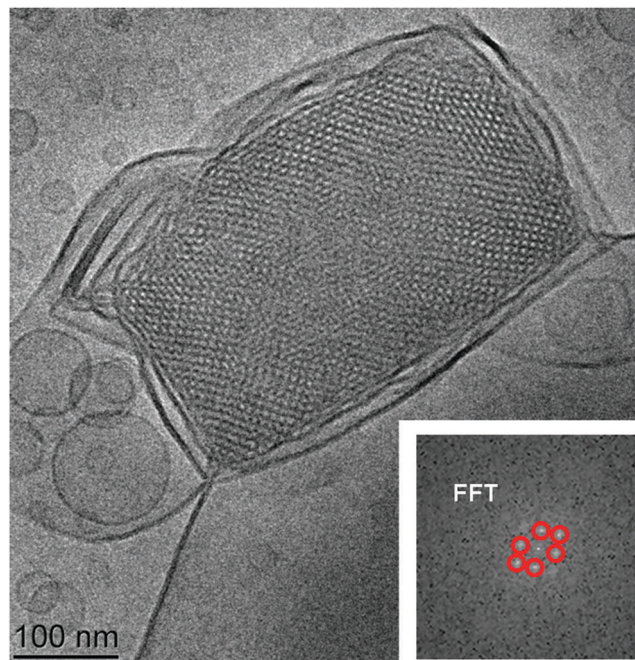
Fig. 3 Cryo-TEM image of a cubosome nanoparticle with traditional (non-swollen) aqueous channels yielding well defined diffraction peaks in the fast Fourier transform (FFT) pattern (inset). The red colour in the inset highlights the FFT image analysis. This nanocarrier does not include a cationic lipid (*i.e.* the particle was obtained at 0 mol% DOMA).
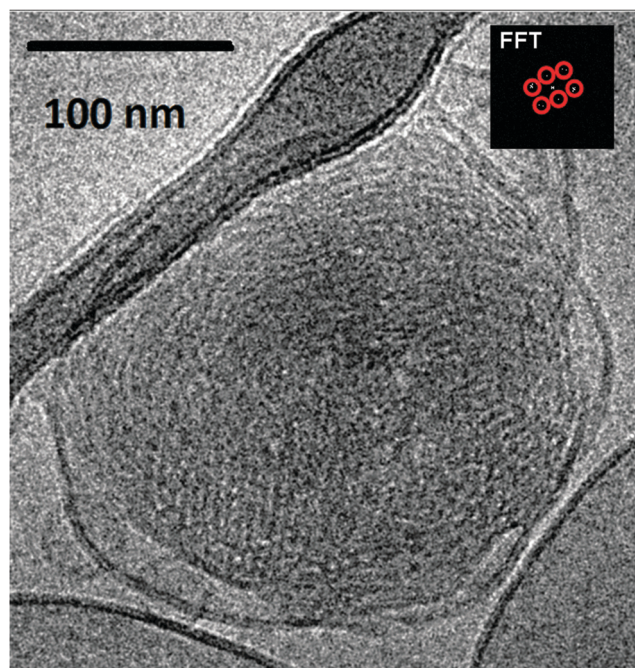

Fig. 4 Cryo-TEM image demonstrating that the reduction of the interfacial charge (10 mol% cationic lipid) may yield liquid crystalline nanoparticles of denser inner packing of the lipid membranes. Vesicular bilayer membranes are present in coexistence with the cubosome lipid nanoparticles at ambient temperature. Depending on the orientation of the nanoparticles with respect to the electron beam, the nanochannel organization may not be laterally well visible.

to the dynamic nature of their inner organization under conditions of full hydration.

In a separate experiment, cubosome particles of a non-swollen (classical cubic lattice) type were obtained in the absence of the cationic lipid component in the self-assembled lipid mixture. The Cryo-TEM image in Fig. 3 shows a well-defined cubic lattice periodicity with a high density of packed nanochannels. This should be favoured by the reduced electrostatic repulsion between the membrane interfaces. The inner cubic symmetry of the LC nanocarrier was clearly detected in the FFT pattern presented in the inset of Fig. 3. Therefore, it may be concluded that the nanochannel topology of the classical PEGylated cubosome particles is similar to that of the uncharged cubosomes stabilized by Pluronic amphiphiles.[9a] The formation of low-curvature vesicle-like membranes at the outer side of the uncharged cubosome particles is likely due to the preferential peripheral localization of the PEG chains of the employed DOPE-PEG$_{2000}$ lipid.

The different densities of the folded lipid membranes inside the swollen and the traditional type cubosome nanoparticles also influenced the morphologies of the nanocarriers found in the Cryo-TEM images. Fig. 4 demonstrates that the reduction of the charge of the lipid/water interfaces leads to the increase of the lipid membrane packing density inside the nanoparticles. As a consequence, the cubic membrane arrangement becomes more perceptibly apparent in the Cryo-TEM images.

The obtained results revealed that the SAXS and Cryo-TEM methods straightforwardly determine the symmetry and the periodicity of the LC nanostructures formed in lipid nanoparticulate samples. Well-defined Bragg peaks of bicontinuous cubic lattices were identified for sufficiently large particles (diameter ∼ 300 nm). Regarding the membrane topology, Conn *et al.*[7a] have interpreted their SAXS data, obtained with a bulk LC phase of the monoelaidin–water mixture, by a lamellar-to-cubic phase transition involving core–shell intermediates of "bulb" onion type. For the nanocarrier system studied here, two complementary structural methods (SAXS and Cryo-TEM) were required in order to evidence, at high resolution, the onion bilayer and the cubic membrane arrangements formed by the amphiphilic building blocks inside the nanoparticle compartments.

Conclusion

In conclusion, it is noteworthy that the immediate recognition of extra-large channel cubosomes by Cryo-TEM imaging might not be straightforward in the absence of structural SAXS data. This may occur because the density of the nanochannels in a single cationic cubic particle of a swollen channel type is essentially reduced as compared to that in a traditional cubic lattice. The lipid membranes in the water-swollen cubic-lattice assembly appear to be fluctuating due to the high membrane flexibility of the extra-large channel compartments. Because of the low channel density in the swollen cubosome intermediates, the obtained Cryo-TEM images may not yield well defined

periodic FFT patterns as those of the traditional (classical) type cubosomes characterized by a high density of tetrahedral-packed nanochannels of small diameters.

A particular advantage of the bicontinuous water-swollen cubic membranes with extra large aqueous channels arises from the fact that they can mimic the topology of bicontinuous membranes found in cellular organelles, for instance that of the endoplasmic reticulum (ER) in eukaryotic cells.[14] The curvature of such membranes can be modulated by embedded membrane proteins, which additionally can tune the diameters of the water channels. This feature may be exploited in future crystallization trials toward the preparation of valuable protein crystals for structure discovery. Moreover, the studied extra-large nanochannel cationic cubosomes may act as potentially efficient nanocarriers for siRNA delivery and mitochondrial targeting.

Experimental

1. Preparation of cationic lipid liquid crystalline nanoparticles with extra large water channels

Cationic liquid crystalline nanoparticles of cubosome-type were prepared by self-assembly in excess of aqueous medium through hydration of a lyophilized mixed lipid film (MO/DOMA/DOPE-PEG$_{2000}$) followed by multiple vortex shaking and agitation cycles in a bath sonicator. The investigated mixed amphiphilic film included the nonlamellar monoglyceride lipid 1-oleoyl-rac-glycerol (MO) (MW 356.55, purity 99.5%, Sigma), the cationic amphiphile dioctadecyldimethylammonium bromide (DOMA) (MW 630.95, purity $\geq$ 99.0%, Selectophore, Fluka), and the PEGylated lipid 1,2-dioleoyl-sn-glycero-3-phosphoethanolamine-N-(methoxy(polyethylene glycol)-2000) ammonium salt (DOPE-PEG$_{2000}$) (MW 2801.51, purity $\geq$ 99.0%, Avanti Polar Lipids). The percentage of the cationic lipid was varied from 0 to 25 mol% at a constant content of the PEGylated lipid (3 mol%). The hydration and dispersion of the lyophilized lipid film was performed in an excess phosphate buffer phase (NaH$_2$PO$_4$/Na$_2$HPO$_4$, 1.10^{-2} M, pH 7, p.a. grade, Fluka). The concentration of the lipid dispersion was 1 wt%. The buffer solution was prepared using MilliQ water (resistivity 18.2 MΩ cm, Millipore Co.). A vortex device and an ultrasonication bath (Branson 2510) were used for sample dispersion and homogenization.

2. Cryogenic transmission electron microscopy (Cryo-TEM)

For Cryo-TEM imaging, liquid samples (2 μL) were dropped on a lacey carbon film covered copper grid (Science Services, Munich, Germany), which was hydrophilized by glow discharge for 15 s. The thin film specimens were instantly shock frozen by rapid immersion into liquid ethane and cooled to approximately 90 K by liquid nitrogen in a temperature-controlled freezing unit (Zeiss Cryobox, Zeiss NTS GmbH, Oberkochen, Germany). After removing ethane, the frozen samples were inserted into a cryo transfer holder (CT3500, Gatan, Munich, Germany) and transferred to a Zeiss EM922 Omega energy-filtered TEM (EFTEM) instrument (Zeiss NTS GmbH, Oberkochen, Germany). The imaging studies were carried out at temperatures around 90 K. The TEM instrument was operated at an acceleration voltage of 200 kV. Zero-loss-filtered images (ΔE = 0 eV) were taken under reduced dose conditions (100–1000 e nm^{-2}). The images were recorded digitally using a bottom-mounted charge-coupled device (CCD) camera system (Ultra Scan 1000, Gatan, Munich, Germany) and combined and processed with a digital imaging processing system (Digital Micrograph GMS 1.8, Gatan, Munich, Germany).

3. Synchrotron radiation small-angle X-ray

Small angle X-ray scattering experiments were performed at the P12 BioSAXS beamline of the European Molecular Biology Laboratory (EMBL) at the storage ring PETRA III of the Deutsche Elektronen Synchrotron (DESY, Hamburg, Germany) at 20 °C using a Pilatus 2M detector (1475 $\times$ 1679 pixels) (Dectris, Switzerland) and synchrotron radiation with a wavelength λ = 1 Å. The sample-to-detector distance was 3 m, and the accessible q-range from 0.006 to 0.35 Å^{-1}. The q-vector was defined as $q = (4\pi/\lambda) \sin \theta$, where 2θ is the scattering angle. The q-range was calibrated using the diffraction patterns of silver behenate. The experimental data were normalized with respect to the incident beam intensity. The background scattering of the solvent buffer was subtracted. The solvent scattering was measured before and after every lipid nanoparticle sample in order to control eventual sample-holder contamination. Eight consecutive frames comprising measurements for the solvent, the sample, and the solvent were acquired. No measurable radiation damage was detected by the comparison of eight successive time frames with 5 s exposure. The final scattering curve was obtained using the program PRIMUS[15a] by averaging the scattering data collected from the measured frames. An automatic sample changer adjusted for a sample volume of 15 μL and a filling cycle of 20 s was used.

4. Fast Fourier transform and azimuthal integration

The ImageJ and pyFAI programs[15b,c] were used for the FFT and the azimuthal integration, respectively. They allow for a versatile treatment and custom implementation of the calibration, background subtraction, and other common tasks of data treatment.

Acknowledgements

References

1 (a) C. Alves, J. S. Pedersen and C. L. P. Oliveira, *J. Appl. Crystallogr.*, 2014, **47**, 84; (b) G. Zhen, T. M. Hinton, B. W. Muir, S. Shi, M. Tizard, K. M. McLean, P. G. Hartley and P. Gunatillake, *Mol. Pharmaceutics*, 2012, **9**, 2450;

(c) A. Angelova, B. Angelov, R. Mutafchieva, S. Lesieur and P. Couvreur, *Acc. Chem. Res.*, 2011, **44**, 147; (d) D. Pozzi, V. Colapicchioni, G. Caracciolo, S. Piovesana, A. L. Capriotti, S. Palchetti, S. De Grossi, A. Riccioli, H. Amenitsch and A. Laganà, *Nanoscale*, 2014, **6**, 2782; (e) A. Zabara, R. Negrini, O. Onaca-Fischer and R. Mezzenga, *Small*, 2013, **9**, 3602; (f) K. Hales, Z. Clen, K. Wooley and D. J. Pochan, *Nano Lett.*, 2008, **8**, 2023.

2 (a) S. M. Sagnella, X. Gong, M. J. Moghaddam, C. E. Conn, K. Kimpton, L. J. Waddington, I. Krodkiewska and C. J. Drummond, *Nanoscale*, 2011, **3**, 919; (b) M. L. Lynch, A. Ofori-Boateng, A. Hippe, K. Kochvar and P. T. Spicer, *J. Colloid Interface Sci.*, 2003, **260**, 404; (c) A. Angelova, B. Angelov, V. M. Garamus, P. Couvreur and S. Lesieur, *J. Phys. Chem. Lett.*, 2012, **3**, 445; (d) B. Angelov, A. Angelova, B. Papahadjopoulos-Sternberg, S. V. Hoffmann, V. Nicolas and S. Lesieur, *J. Phys. Chem. B*, 2012, **116**, 7676; (e) E. Nazaruk, M. Szlęzak, E. Górecka, R. Bilewicz, Y. M. Osornio, P. Uebelhart and E. M. Landau, *Langmuir*, 2014, **30**, 1383.

3 (a) M. J. Moghaddam, L. de Campo, L. J. Waddington, A. Weerawardena, N. Kirby and C. J. Drummond, *Soft Matter*, 2011, **7**, 10994; (b) A. Angelova, B. Angelov, B. Papahadjopoulos-Sternberg, C. Bourgaux and P. Couvreur, *J. Phys. Chem. B*, 2005, **109**, 3089; (c) M. G. Lara, M. V. L. B. Bentley and J. H. Collett, *Int. J. Pharm.*, 2005, **293**, 241; (d) A. Angelova, B. Angelov, M. Drechsler and S. Lesieur, *Drug Discovery Today*, 2013, **18**, 1263; (e) A. Angelova, B. Angelov, M. Drechsler, V. M. Garamus and S. Lesieur, *Int. J. Pharm.*, 2013, **454**, 625; (f) N. Carlsson, N. Sanandaji, M. Voinova and B. Åkerman, *Langmuir*, 2006, **22**, 4408; (g) F. Muller, A. Salonen and O. Glatter, *Colloids Surf., A*, 2010, **358**, 50.

4 (a) L. Qin, I. Kufareva, L. G. Holden, C. Wang, Y. Zheng, C. Zhao, G. Fenalti, H. Wu, G. W. Han, V. Cherezov, R. Abagyan, R. C. Stevens and T. M. Handel, *Science*, 2015, **347**, 1117; (b) L. Hosta-Rigau, Y. Zhang, B. M. Teo, A. Postma and B. Städler, *Nanoscale*, 2013, **5**, 89; (c) A. Zabara and R. Mezzenga, *Soft Matter*, 2012, **8**, 6535; (d) A. B. Wöhri, L. C. Johansson, P. Wadsten-Hindrichsen, W. Y. Wahlgren, G. Fischer, R. Horsefield, G. Katona, M. Nyblom, F. Öberg, G. Young, R. J. Cogdell, N. J. Fraser, S. Engström and R. Neutze, *Structure*, 2008, **16**, 1003.

5 (a) Y.-K. Gong and F. M. Winnik, *Nanoscale*, 2012, **4**, 360; (b) Y. Wang and F. Li, *Adv. Mater.*, 2011, **23**, 2134; (c) S. T. Hyde, *Langmuir*, 1997, **13**, 842; (d) G. E. Schröder-Turk, L. de Campo, M. E. Evans, M. Saba, S. C. Kapfer, T. Varslot, K. Grosse-Brauckmann, S. Ramsden and S. T. Hyde, *Faraday Discuss.*, 2013, **161**, 215.

6 (a) M. Rappolt, G. M. Di Gregorio, M. Almgren, H. Amenitsch, G. Pabst, P. Laggner and P. Mariani, *Europhys. Lett.*, 2006, **75**, 267; (b) A. Angelova, B. Angelov, B. Papahadjopoulos-Sternberg, M. Ollivon and C. Bourgaux, *J. Drug Delivery Sci. Technol.*, 2005, **15**, 108; (c) B. Angelov, A. Angelova, V. M. Garamus, M. Drechsler, R. Willumeit, R. Mutafchieva, P. Štěpánek and S. Lesieur, *Langmuir*, 2012, **28**, 16647; (d) J. G. Petrov and A. Angelova, *Langmuir*, 1992, **8**, 3109; (e) C. Nilsson, J. Østergaard, S. W. Larsen, C. Larsen, A. Urtti and A. Yaghmur, *Langmuir*, 2014, **30**, 6398.

7 (a) C. E. Conn, O. Ces, X. Mulet, S. Finet, R. Winter, J. M. Seddon and R. Templer, *Phys. Rev. Lett.*, 2006, **96**, 1; (b) J. Lee, S.-U. Choi, M.-K. Yoon and Y. W. Choi, *Arch. Pharmacal Res.*, 2003, **26**, 880; (c) M. Buchanan, S. U. Egelhaaf and M. E. Cates, *Colloids Surf., A*, 2001, **185**, 293; (d) V. Babin and A. Ciach, *J. Chem. Phys.*, 2003, **119**, 6217; (e) M. Nakano, A. Sugita, H. Matsuoka and T. Handa, *Langmuir*, 2001, **17**, 3917.

8 (a) B. Angelov, A. Angelova, S. Filippov, M. Drechsler, P. Štěpánek and S. Lesieur, *ACS Nano*, 2014, **8**, 5216; (b) B. Angelov, A. Angelova, S. K. Filippov, T. Narayanan, M. Drechsler, P. Štěpánek, P. Couvreur and S. Lesieur, *J. Phys. Chem. Lett.*, 2013, **4**, 1959; (c) B. Angelov, A. Angelova, M. Ollivon, C. Bourgaux and J. Campitelli, *J. Am. Chem. Soc.*, 2003, **125**, 7188; (d) T. Landh, *J. Phys. Chem.*, 1994, **98**, 8453; (e) J. Gustafsson, T. Nylander, M. Almgren and H. Ljusberg-Wahren, *J. Colloid Interface Sci.*, 1999, **211**, 326; (f) J. Engblom, Y. Miezis, T. Nylander, V. Razumas and K. Larsson, *Prog. Colloid Polym. Sci.*, 2000, **116**, 9; (g) R. Winter, J. Erbes, R. H. Templer, J. M. Seddon, A. Syrykh, N. A. Warrender and G. Rapp, *Phys. Chem. Chem. Phys.*, 1999, **1**, 887; (h) H. M. G. Barriga, A. I. I. Tyler, N. L. C. McCarthy, E. S. Parsons, O. Ces, R. V. Law, J. M. Seddon and N. J. Brooks, *Soft Matter*, 2015, **11**, 600; (i) T. A. Balbino, A. A. M. Gasperini, C. L. P. Oliveira, A. R. Azzoni, L. P. Cavalcanti and L. G. de La Torre, *Langmuir*, 2012, **28**, 11535.

9 (a) J. Barauskas, M. Johnsson, F. Joabsson and F. Tiberg, *Langmuir*, 2005, **21**, 2569; (b) T. S. Awad, Y. Okamoto, S. M. Masum and M. Yamazaki, *Langmuir*, 2005, **21**, 11556; (c) X. Mulet, X. Gong, L. J. Waddington and C. J. Drummond, *ACS Nano*, 2009, **3**, 2789; (d) B. Angelov, A. Angelova, B. Papahadjopoulos-Sternberg, S. Lesieur, J.-F. Sadoc, M. Ollivon and P. Couvreur, *J. Am. Chem. Soc.*, 2006, **128**, 5813; (e) S. Murgia, S. Bonacchi, A. M. Falchi, S. Lampis, V. Lippolis, V. Meli, M. Monduzzi, L. Prodi, J. Schmidt, Y. Talmon and C. Caltagirone, *Langmuir*, 2013, **29**, 6673.

10 (a) B. W. Muir, G. Zhen, P. Gunatillake and P. G. Hartley, *J. Phys. Chem. B*, 2012, **116**, 3551; (b) C. Moitzi, S. Guillot, G. Fritz, S. Salentinig and O. Glatter, *Adv. Mater.*, 2007, **19**, 1352; (c) I. M. S. C. Oliveira, J. P. N. Silva, E. Feitosa, E. F. Marques, E. M. S. Castanheira and M. E. C. D. R. Oliveira, *J. Colloid Interface Sci.*, 2012, **374**, 206; (d) Q. Liu, Y.-D. Dong, T. L. Hanley and B. J. Boyd, *Langmuir*, 2013, **29**, 14265; (e) A. Angelova, B. Angelov, R. Mutafchieva and S. Lesieur, *J. Inorg. Organomet. Polym.*, 2015, **25**, 214; (f) B. Angelov, A. Angelova, R. Mutafchieva, S. Lesieur, U. Vainio, V. M. Garamus, G. V. Jensen and J. S. Pedersen, *Phys. Chem. Chem. Phys.*, 2011, **13**, 3073.

11 (a) A. Yaghmur, P. Laggner, M. Almgren and M. Rappolt, *PLoS One*, 2008, **3**, e3747; (b) B. Angelov, A. Angelova, S. K. Filippov, G. Karlsson, N. Terrill, S. Lesieur and P. Štěpánek, *Soft Matter*, 2011, **7**, 9714; (c) M. M. A. E. Claessens, B. F. van Oort, F. A. M. Leermakers, F. A. Hoekstra and M. A. Cohen Stuart, *Biophys. J.*, 2004, **87**, 3882; (d) M. Uyama, M. Nakano, J. Yamashita and T. Handa, *Langmuir*, 2009, **25**, 4336;

(e) A. Yaghmur, B. Sartori and M. Rappolt, *Phys. Chem. Chem. Phys.*, 2011, **13**, 3115.

12 (a) A. Angelova, C. Ringard-Lefebvre and A. Baszkin, *J. Colloid Interface Sci.*, 1999, **212**, 275; (b) J. G. Petrov, D. Mobius and A. Angelova, *Langmuir*, 1992, **8**, 201; (c) J. G. Petrov, A. Angelova and D. Mobius, *Langmuir*, 1992, **8**, 206; (d) A. Angelova, C. Ringard-Lefebvre and A. Baszkin, *J. Colloid Interface Sci.*, 1999, **212**, 280.

13 P. Heftberger, B. Kollmitzer, F. A. Heberle, J. Pan, M. Rappolt, H. Amenitsch, N. Kucerka, J. Katsaras and G. Pabst, *J. Appl. Crystallogr.*, 2014, **47**, 173.

14 (a) Z. A. Almsherqi, T. Landh, S. D. Kohlwein and Y. Deng, *Int. Rev. Cell Mol. Biol.*, 2009, **274**, 275; (b) A. Sesso, F. P. De Faria, E. S. Miazato Iwamura and H. J. Corrêa, *Cell Sci.*, 1994, **107**, 517.

15 (a) P. V. Konarev, V. V. Volkov, A. V. Sokolova, M. H. J. Koch and D. I. Svergun, *J. Appl. Crystallogr.*, 2003, **36**, 1277; (b) M. Noguchi, H. Kikuchi, M. Ishibashi and S. Noda, *Br. J. Cancer*, 2003, **88**, 195–201; (c) J. Kieffer and D. Karkoulis, *J. Phys.: Conf. Ser.*, 2013, **425**, 202012; (d) M. Clerc and E. Dubois-Violette, *J. Phys. II*, 1994, **4**, 275–286; (e) P. Garstecki and R. Holyst, *Langmuir*, 2002, **18**, 2529.